2008－CVIM－164 (4)
2008／9／5

レイリー散乱による天空光の偏光解析および魚眼カメラによる太陽方向推定

宮崎 大輔† Mahdi Ammar‡ 川上 玲† 池内 克史†

†東京大学 生産技術研究所

‡Ecole Supérieure de Physique et de Chimie Industrielles

あらまし 近年，バーチャルアースやグーグルアース，マップキューブなど，屋外環境をモデル化して仮想都市を作ったり，そこに他の仮想物体を合成するサービスが盛んに展開されている．本稿では，屋外環境の解析の第一歩として，屋外環境の情報の半分を占める天空光の偏光解析の結果について報告する．太陽光は非偏光であるが，大気中のエアロゾルに太陽光が反射することにより，空が偏光する．本稿では，直線偏光板と魚眼レンズを搭載したカメラで天空を観測し，晴天時および曇天時において太陽の方向を検出した実験結果を示し，その考察を行う．

Polarization analysis of the skylight caused by Rayleigh scattering and sun orientation estimation using fisheye-lens camera

Daisuke Miyazaki†, Mahdi Ammar‡, Rei Kawakami†, and Katsushi Ikeuchi†

†Institute of Industrial Science, The University of Tokyo

‡Ecole Supérieure de Physique et de Chimie Industrielles

Abstract Recently, Virtual Earth, Google Earth, or Map Cube provide a virtual city modeled from real outdoor environment, and they also provide a service to embed other virtual objects into the virtual space. For the first step for analyzing such complex outdoor scene, we show some results of analyzing the skylight, which dominates the half of the outdoor scene. The sunlight is unpolarized, and the sky becomes polarized when the sunlight is reflected at the aerosol. We provide some experimental results of detecting the sun orientation under clear sky and cloudy sky, using linear polarizer and fisheye lens.

1. Introduction

The mathematical and physical description of the state of polarization of sunlight scattered in and transmitted through the Earth's atmosphere is a difficult problem. In the past, many theoretical calculations and computer simulations of the atmospheric radiative transfer focused on the polarization characteristics of the clear, cloudy and overcast sky [1, 2]. The intensity, the degree and the angle of polarization patterns of the sky has been the subject of many theoretical and experimental studies, because the understanding of these optical characteristics was one of the most interesting and important problems in atmospheric optics, in metrology and in polarization-sensitive animals.

Most ground-level measurements of the skylight polarization were performed by means of point-source polarimeters for different wavelengths of light. As these polarimeters possess a very small aperture ($3 \sim 5°$), the polarization characteristics of the sky can only be analyzed within a very restricted field of view. Recently, the polarization sky patterns were measured using 180° (full-sky) imaging polarimetry in the red, green and blue spectral ranges [1–3]. This system uses a photo-emulsion and requires a digitalization of the images, which is considered nowadays as expensive and time-consuming process. Since we use a digital camera, our sky imaging polarimeter is more efficient.

In the first half of this paper, we show the measurement results of the sky polarization patterns under different sky conditions (clear, cloudy, and overcast sky). In the second half, we show the measurement results when the camera orientation is not vertical to the ground.

2. Materials and methods

2.1. Measurement of the celestial polarization pattern using sky imaging polarimetry

Our polarimetric measurements were performed in Tokyo, The University of Tokyo, Institute of Industrial Science (35°40′ N, 139°40′ E), in different dates in June and July 2008, one or two hours before the Sunset. The set-up of our full-sky imaging polarimetry is shown in Fig. 1. The technique used here is similar to the technique used in the latest publications [1–3,5]. The detector was a digital sensor of a DSLR (digital single-lens reflex) camera (Canon EOS 5D): the maxima and half-bandwidths of its spectral sensitivity curves were: red=620 ± 50 nm, green=530 ± 30 nm, blue=470 ± 30 nm. The fish-eye lens (Sigma EX DG Fish-eye, F=3.5, focal length 8 mm) ensures an angle of view of 180°. The polarizing filter (Kenko PL, 72 mm) enables the measurement of the sky polarization patterns. However, using a commercial DSLR camera, it was imperative to set up the polarizing filter in front of the fish-eye lens. Hence, our imaging polarimeter allowed only an angle of view of 130°. Using a personal computer and Canon software (EOS utility), three photographs were taken for three different alignments of the transmission axis of the polarizer (0, 45°, and 90° clockwise from the top view of the camera). The polarizer was rotated manually (Fig. 1). The initial position of the camera was set up on a tripod such that its axis passing through the view-finder pointed northwards and the optical axis of the fish-eye lens was vertical. The three-dimensional celestial hemisphere was represented in two dimensions by a polar-coordinate system, where the zenith angle θ and the azimuth angle φ from the camera top view axis (x-axis) are measured radially and tangentially, respectively (Fig. 2). In this two-dimensional coordinate system, the zenith is at the origin and 65° of the zenith-axis corresponds to the outermost circle.

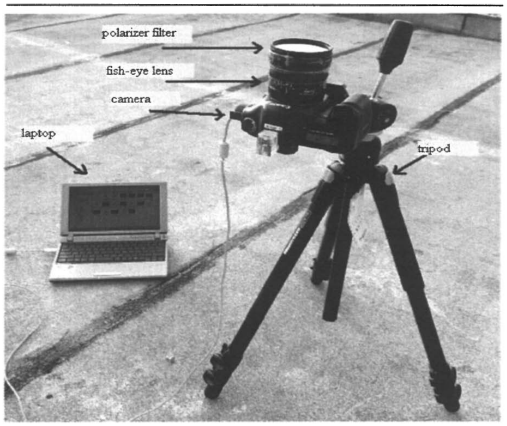

Fig. 1: Imaging polarimetry system (linear polarizer, fish-eye lens, Canon camera, tripod, and a laptop).

2.2. Polarization calculations using the single-scattering Rayleigh model

Light radiated by the Sun is unpolarized, however, on its way through the earth's atmosphere, sunlight is scattered by the air molecules, i.e., by particles much smaller than the wavelength. Sunlight remains unpolarized if it reaches the observer directly (scattering angle 0°), but is linearly polarized if it is scattered by atmospheric O_2 and N_2 molecules. Within a theoretical (Rayleigh) atmosphere, the degree of polarization reaches 100%, if the scattering angle is 90°. Other scattering angles yield smaller degrees of polarization. The light is then said to be partially linearly polarized (Fig. 3).

This scattering results in the polarization of light: the electric E-vector is oriented perpendicularly to the plane of scattering formed by the Sun, the observed point and the observer (Fig. 4 (A)). Consequently, the E-vectors in the sky form concentric circles around the Sun. A circle C_γ is described by the following equation:

$$\cos\gamma = \sin\theta_s \sin\theta \cos\psi - \sin\theta \cos\theta_s \qquad (1)$$

where γ is the angular distance between the observed celestial point and the Sun, θ_s is the solar zenith angle, and θ and ψ are the angular distances of the observed point from the zenith and the solar meridian, respectively (Fig. 4 (A)). From geometrical consideration, the E-vector orientation from the local meridian is expressed as:

$$\tan\alpha = \frac{d\varphi}{d\theta} = \frac{\cos\theta \sin\theta_s \cos\psi - \sin\theta \cos\theta_s}{\sin\theta \sin\theta_s \sin\psi} \qquad (2)$$

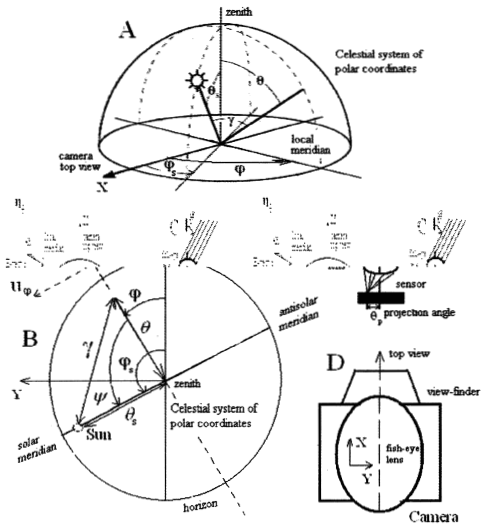

Fig. 2: Three (A) and two dimensional (B) representation of the celestial polar coordinates system used in the representation of the sky polarization patterns. (C) Schematic representation of the relationship between the off-axis angle θ and the projection angle θ_p projected onto the digital sensor by the fish-eye lens. Ideally: $\theta_p = \theta$. (D) Schematic representation of the camera: a clockwise angle from the top view of the camera becomes a counterclockwise angle on the photo.

Fig. 4 reveals yet another skylight phenomenon, depicted by the size of the black lines. Apart from the orientation α of the E-vector, it is also the degree of polarization d that varies across the celestial hemisphere. According to the Rayleigh theory, d depends on the scattering angle γ such that:

$$d = 100\frac{I_{\text{polarized}}}{I_{\text{total}}} = 100\frac{\sin^2\gamma}{1+\cos^2\gamma} \qquad (3)$$

and Eq. (1). d varies from 0 ($\gamma = 0°$) to 100% ($\gamma = 90°$).

2.3. Data processing and analysis

In order to analyze the skylight patterns, we calculated the intensity I, degree of polarization d, and E-vector orientation α. This polarization analysis was based on Stokes parameters for partially polarized light [12]. It is worth noticing that the light in the atmosphere is not circularly polarized [9], so we do not need to evaluate this quantity

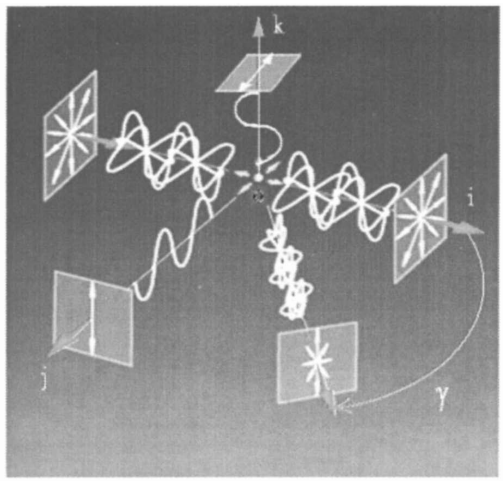

Fig. 3: Polarization arising from light scattering within the earth's atmosphere. Unpolarized sunlight remains unpolarized if the scattering angle is 0°. The degree of polarization reaches 100%, if the scattering angle is 90°. Other scattering angles yield smaller degrees of polarization.

(i.e. we assume that the light in the atmosphere is partially *linearly* polarized).

In short, if I_0, I_{45}, and I_{90} represent the intensity values recorded when the polarizing filter is at 0°, 45°, and 90° from the camera top view, respectively, then, from geometrical considerations, the orientation of polarization α' (representing the E-vector shift from the top view) is given by:

$$\alpha' = \frac{1}{2}\arctan\left(\frac{I_0 + I_{90} - 2I_{45}}{I_{90} - I_0}\right) \qquad (4)$$

We use the following α'' which is scaled between $-90°$ and 90°.

$$\alpha'' = \begin{cases} \alpha' & (I_{90} < I_0) \\ \alpha' + 90° & (I_{90} \geq I_0) \wedge (I_{90} + I_0 < 2I_{45}) \\ \alpha' - 90° & (I_{90} \geq I_0) \wedge (I_{90} + I_0 \geq 2I_{45}) \end{cases} \qquad (5)$$

Finally, α was expressed as an angle drifted from the local meridian, in order to analyze the E-vector orientation patterns independently of the initial position of the polarizer such that (Fig. 2):

$$\alpha = \alpha'' - \varphi \qquad (6)$$

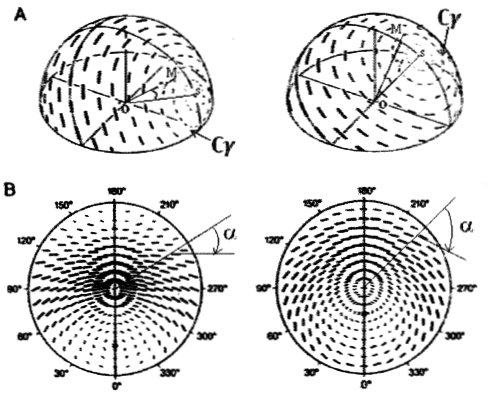

Fig. 4: Three (A) and two dimensional (B) representation of the pattern of polarized light in the sky depicted for two different elevations of the Sun (left: $\theta_s = 65°$, right: $\theta_s = 25°$). The orientation and the size of the black mark represent the direction (α) and the degree of polarization (d), respectively.

The total intensity is given by:

$$I = I_0 + I_{90}\,, \tag{7}$$

while the degree of polarization is given by:

$$d = 100\frac{\sqrt{(I_0 + I_{90})^2 + (I_0 + I_{90} - 2I_{45})^2}}{I_0 + I_{90}}\,. \tag{8}$$

2.4. Neutral points

Rayleigh's explanation of the polarization of clear-sky would predict that light is unpolarized in the direction of the Sun or anti-Sun, whichever is above the horizon. But observations had already demonstrated the existence of three unpolarized directions: above the Sun (the Babinet point), below the Sun (the Brewster point) and above the anti-Sun (the Arago point), and hinted at a fourth point below the anti-Sun (Fig. 5). The deviation from the Sun and anti-Sun is interpreted as a multiple-scattering effect, which splits the unpolarized points of the single-scattering theory into two points; this phenomenon has been considerably elaborated [8]. These unpolarized points typically lie within $15 \sim 35°$ of the Sun or anti-Sun. The positions of the neutral points are also strongly modified by clouds, atmospheric turbidity and the intensity of air pollution. The region between the Sun and the horizon is the brightest area of the sky, and haze near the horizon yields generally low polarization values, so that the Brewster point is very difficult to observe. Since the fourth neutral point is always under the horizon, only the Babinet and Arago points could be seen unambiguously.

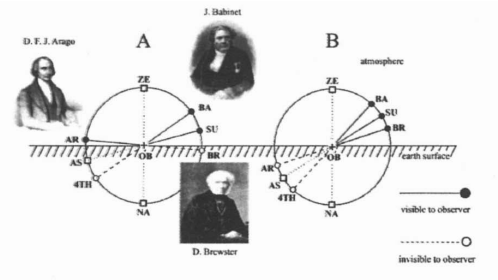

Fig. 5: Schematic diagram showing the normal positions of the Arago (AR), Babinet (BA), and Brewster (BR) neutral points of skylight polarization in the vertical plane including the ground-level observer (OB), Sun (SU), zenith (ZE), anti-solar point (AS), and nadir (NA). From the ground, only two neutral points are visible simultaneously: either the Arago and Babinet points (A, for lower solar elevations), or the Babinet and Brewster points (B, for higher solar elevations).

2.5. Polarization measurements using a camera in general position

All the recent studies of the sky polarization patterns [1–3] were performed using a camera sensor set up in the horizontal plane (i.e. the optical axis of the fish-eye lens was vertical to the ground). This condition is considered as a serious limitation if we try to apply the latest method in the field of Computer Vision. Hence, it is worth investigating the sky polarization patterns using a camera in general position (i.e. the optical axis of the fish-eye lens is not necessarily vertical). Using a tripod, it is possible to rotate the camera top-view (x-axis) from the north (φ_{camera}), and to rotate the optical axis of the fish-eye lens (z-axis) around the x-axis of the camera reference (x, y, z).

To simulate the sky polarization patterns using the Rayleigh single-scattering model (Eq. (2)), the coordinates of the Sun (θ_s', φ_s') in the new camera reference (x, y', z') are the only required parameters: $\mathbf{OS}' = R(x, \theta_i) \cdot \mathbf{OS}$ where $R(x, \theta_i)$ is the rotation matrix around x-axis by angle θ_i, $\mathbf{OS}$ and $\mathbf{OS}'$ are the Sun coordinate

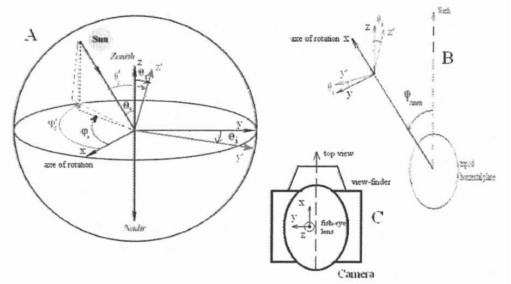

Fig. 6: (A) The Sun coordinates in the camera reference (x, y, z) while the optical axis of the fish-eye lens, and after rotation of camera around the x-axis in the reference (x, y', z'). (B) The camera orientation from the North. (C) Schematic representation of the camera and the camera reference (x, y, z).

vectors in (x, y, z) and (x, y', z'), respectively (Fig. 6).

In detail:

$$\begin{bmatrix} \sin\theta'_s \cos\varphi'_s \\ \sin\theta'_s \sin\varphi'_s \\ \cos\theta'_s \end{bmatrix} = \begin{bmatrix} 1 & 0 & 0 \\ 0 & \cos\theta_i & -\sin\theta_i \\ 0 & \sin\theta_i & \cos\theta_i \end{bmatrix} \begin{bmatrix} \sin\theta_s \cos\varphi_s \\ \sin\theta_s \sin\varphi_s \\ \cos\theta_s \end{bmatrix} \quad (9)$$

Therefore, the Sun coordinates (θ_s, φ_s) in the horizontal plane could be determined from (θ'_s, φ'_s) by the following equations:

$$\begin{cases} \sin\theta_s \cos\varphi_s \\ = \sin\theta'_s \cos\varphi'_s & \text{(I)} \\ \sin\theta_s \sin\varphi_s \\ = \cos\theta_i \sin\theta'_s \sin\varphi'_s + \sin\theta_i \cos\theta'_s & \text{(II)} \\ \cos\theta_s \\ = -\sin\theta_i \sin\theta'_s \cos\varphi'_s + \cos\theta_i \cos\theta'_s & \text{(III)} \end{cases} \quad (10)$$

3. Results

3.1. Polarization sky patterns

We measured the patterns of the degree of linear polarization d, and the angle of polarization of a clear sky by our sky imaging polarimetry in the red 650 nm, green 550 nm, and blue 450 nm parts of the spectrum.

As expected, d from the clear sky was highest at 90° from the Sun and gradually decreased toward the solar and

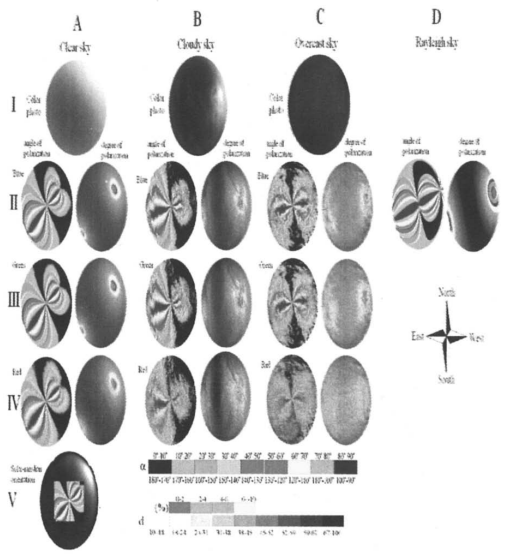

Fig. 7: Color picture (I), degree of linear polarization d (II–IV, right), and angle of polarization α (II–IV, left) calculated clockwise from the local meridian were measured by full-sky imaging polarimetry in the red (650 nm), green (550 nm), and blue (450 nm) parts of the spectrum in different sky conditions (clear sky (A), cloudy sky (B), overcast sky (C)). For the clear sky (A-V), the solar-meridian orientation was determined with an excellent precision. (D) Patterns of the degree and angle of polarization of skylight calculated using the single-scattering Rayleigh model. The optical axis of the fish-eye lens was vertical and the center of the circular patterns is the zenith.

antisolar points (Fig. 7 (A)). Furthermore, d was highest in the red ($d_{\max} = 65\%$) and lowest in the blue ($d_{\max} = 39\%$) part of the spectrum (Table 1).

The angle of polarization of light from the clear sky had a characteristic pattern (Fig. 7 (A)): the isolines with constant were always eight-shaped with a center at the zenith and an axis of mirror symmetry coinciding with the solar-antisolar meridian in such a way that the smaller loop of the eight figure was always in the solar half of the sky.

Comparison of the measured (Fig. 7 (A)) and theoretical (Fig. 7 (D)) patterns indicates that, apart from regions near the Sun and anti-Sun, the simple single-scattering Rayleigh theory describes the characteristics of the sky

Table 1: The degree of linear polarization d (average $\pm$ standard deviation) is averaged over the entire sky for different skies conditions.

	Degree of linear polarization (%)		
	Clear sky	Cloudy sky	Overcast sky
Blue	32 ± 12	17 ± 6	12 ± 6
Green	31 ± 12	15 ± 5	10 ± 5
Red	34 ± 14	15 ± 7	10 ± 7

polarization patterns relatively well. The most striking differences between the actual and the theoretical patterns are the consequences of the neutral (unpolarized) points. In the single-scattering Rayleigh model, such neutral points do not occur; or rather coincide with the anti-Sun and the Sun. Because of these neutral points, the isolines belonging to given values of the degree and angle of polarization differ more or less from each other in the real and the Rayleigh sky.

Fig. 7 (B) and Fig. 7 (C) represent the patterns of the degree and angle of polarization of partially cloudy and overcast skies measured again in the blue, green and red spectral ranges. For the cloudy sky, one can notice from Fig. 7 (B) that the degree of polarization is strongly reduced in those regions of the sky in which clouds appear. Moreover, the degree of polarization d of light from the overcast sky was very low due to the strong multiple scattering of light on the cloud particles (Fig. 7 (C)). The maximum of d ranged between 13% and 18% and it is almost independent on the wavelength (Table 1). The most outstanding observation is that the angle of polarization of both cloudy and overcast sky were qualitatively the same as those of the clear sky (Fig. 7 (B) and Fig. 7 (C)): the isolines were again eight shaped with a center at the zenith and a symmetry axis along the solar-antisolar meridian. This observation is in accordance with previous results [1].

The Arago and Babinet neutral points belong to the solar-antisolar meridian and the so-called neutral line. As shown in Fig. 7 (A-V), the neutral line points the Sun orientation (Sun Azimuth) with an excellent precision (less than 3° of error) for the clear sky. For overcast sky, the Sun orientation was determined within 10° of precision. (When the Sun is occulted by clouds, we used the solar position calculator [11] (`http://aa.usno.navy.mil`) to determine the Sun orientation from the North, using the Date Picture Taken (Date-time of the picture) and the exact position of camera (longitude and latitude on the earth)).

Nevertheless the angle of polarization patterns does not give the exact position of the Sun (Sun Elevation). The Sun Elevation could be approximately determined using an empirical relationship between the neutral points and the Sun position ($\theta_s = \theta_{\text{Babinet}} + 30°, \theta_s = \theta_{\text{Arago}} + 20°$, for the blue in clear sky condition [5]).

3.2. Application in computer vision

A pilot experience was performed to check out experimentally the theoretical study described previously (Section 2.5). The optical axis of the fish-eye lens was set up at 35° from the vertical (Fig. 6; $\theta_i = -35°$). The camera was rotated progressively 15° counterclockwise from the North (around the z-axis of the tripod, Fig. 6).

As shown in Fig. 8, the angle α and the degree of polarization d present similar patterns with those shown in Fig. 7 (taken while the optical axis of the fish-eye lens was vertical). Although, the α-patterns are always eight-shaped; the Arago, the Babinet and the center of the circular patterns does not form a line anymore. The equations (I, II, III) could be used to determine the solar meridian orientation φ_s from the North by measuring the Babinet (or the Arago) coordinates (θ'_b, φ'_b) (since $\varphi_s = \varphi_{\text{Babinet}} = 180° + \varphi_{\text{Arago}}$). To evaluate the accuracy of this method, the Babinet (or the Arago) coordinates (θ'_b, φ'_b) were measured from the images (Fig. 8 (B) and Fig. 8 (C)) and compared to the Babinet coordinates (θ_b, φ_b) in the horizontal plane measured from the image (Fig. 8 (A)) by using the following ratios (R_1, R_2, R_3) derived from the equations (I, II, III):

$$\begin{cases} R_1 = \dfrac{\sin\theta'_b \cos\varphi'_b}{\sin\theta_b \cos\varphi_b} \\ R_2 = \dfrac{\cos\theta_i \sin\theta'_b \sin\varphi'_b + \sin\theta_i \cos\theta'_b}{\sin\theta_b \sin\varphi_b} \\ R_3 = \dfrac{-\sin\theta_i \sin\theta'_b \sin\varphi'_b + \cos\theta_i \cos\theta'_b}{\cos\theta_b} \end{cases} \tag{11}$$

All those ratios should be equal to one if this method was accurate. We found that the equations (I and III) are very accurate; however the equation II seems to be instable and very sensitive to the errors of measurements (Fig. 9). (Although the reason of this instability still un-

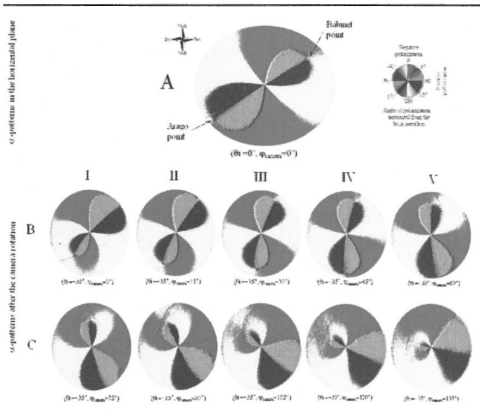

Fig. 8: (A) The angle of polarization patterns of the sky measured while the optical axis of the fish-eye lens was vertical. (B–C) The angles of polarization patterns of the sky measured after rotation of the optical axis of the fish-eye lens ($-35°$) from the vertical around the x-axis of the camera, and progressive rotation of the camera from the North by $15°$ around the vertical (z-axis) of the tripod (Fig. 6). The positions of the Arago and Babinet neutral (unpolarized) points are marked by black and white circles, respectively.

known for us, the equation II is certainly the most complex, requiring all the parameters).

Fortunately, the problem could be solved using only two equations (I, III). Therefore, the solar meridian orientation could be evaluated accurately using the Babinet or the Arago neutral point coordinates and the equations (I, III). Finally, the exact Sun position could be determined using the method described previously (Section 3.1).

4. Discussion

4.1. Polarization sky patterns

In the past, the degree d and angle α of linear polarization of the sky patterns were widely studied theoretically as well as experimentally, because the understanding of these optical characteristics of the sky was one of the most interesting and important problems in atmospheric optics and in polarization sensitive animals.

As the unpolarized sunlight enters the Earth's atmosphere, it is Rayleigh-scattered by the air, the consequence of which is that it becomes partially linearly polarized.

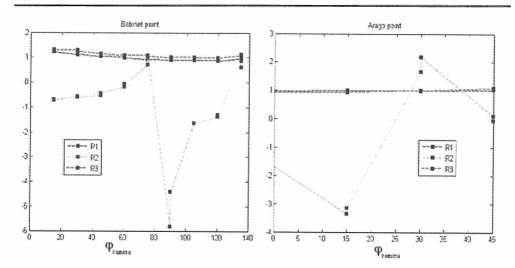

Fig. 9: The accuracy of the determination of the solar meridian orientation using the Babinet and Arago neutral points and the equations (I, II, III). The ratios R_1, R_2 and R_3 were calculated using the measurements of the Babinet and the Arago coordinates from the images (Fig. 8). Those ratios should be equal to one if the equations (I, II, III) were accurate.

According to our measurements (Fig. 7 (A)), the polarization patterns of the clear sky are definitely described by the Rayleigh model. However, around the Sun and the anti-Sun where the neutral points occur, the E-vector pattern differs considerably from the Rayleigh pattern because of the negative polarization caused by the multiple scattering.

For the cloudy and overcast sky, due to the strong multiple scattering on the particles (ice crystals or water droplets) of thick clouds, the direction of polarization of light does not follow logically the single-scattering Rayleigh model. We found that the pattern of the angle of polarization α of the overcast sky (Fig. 7 (B) and Fig. 7 (C)) is qualitatively the same as that of the clear sky (a symmetry axis coinciding with the solar-antisolar meridian, the smaller loop of the eight-shape point the solar half of the sky). Therefore, the solar meridian orientation could be determined from the angle α of polarization patterns in all the atmosphere conditions, especially if the Sun is occulted by clouds or located outside the camera field of view. These results are of great importance for the orientation of polarization-sensitive animals and human navigation (e.g., in aircraft flying near the geomagnetic poles and using a polarization sky compass).

Finally, according to our measurements, the only qualitative difference among clear, partly cloudy, and totally overcast skies is in the degree of linear polarization d: the highest the degree of polarization, the clearest the sky is.

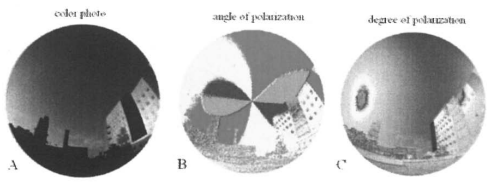

Fig. 10: (A) Color photo of an outdoor scene (Institute of Industrial Science, The University of Tokyo), (B) angle of polarization pattern: the smaller loop of the eight-shape point roughly the solar meridian direction in the photo, (C) degree of polarization pattern.

This feature is useful for the estimation of the atmosphere condition (clear, foggy, cloudy, smoky, or overcast sky).

4.2. Applications in computer vision

To our knowledge, this is the first attempt to apply the polarization sky patterns in Computer Vision. We present here an accurate method to determine the solar meridian orientation from photos taken in the outdoor, using a polarizing filter, while only small part of the sky is available and the camera sensor is not horizontal.

For instance in Fig. 10, the solar meridian orientation could be determined from photos of an outdoor scene using the angle of polarization pattern even if the eight-shape is not complete. And so, the orientation of the camera could be determined from the solar meridian. Hence, knowing the Date Picture Taken (date and time when the picture was taken) and the exact position of the camera (longitude and latitude on the earth), and using a solar position calculator [11], the camera orientation from the North could be also evaluated. This is of great importance for orientation purpose in Computer Vision. (For example, 3D-modeling of outdoor objects, etc.)

This method enables, also, the evaluation of the Sun orientation in the photo, and so the distinction between the sunlight and the skylight could be performed unambiguously in an outdoor scene (Fig. 10 (B)). This is of great importance in photometric and image analysis where the localization of the light source is usually a mean issue.

Finally, using the degree of polarization patterns (Fig. 10 (C)), the sky condition in the photo (clear, foggy, cloudy, or overcast sky) could be determined precisely, and knowing the Sun position (by applying the previous method), the outdoor scene appearance could be simulated under different atmosphere conditions.

Acknowledgment

This research was supported in part by the Ministry of Education, Culture, Sports, Science and Technology under the Leading Project, "Development of High Fidelity Digitization Software for Large-Scale and Intangible Cultural Assets." This work was performed while Mahdi Ammar was an intern at The University of Tokyo (2008.4–7).

References

[1] Hegedüs *et al.*, "Polarization patterns of thick clouds: overcast skies have distribution of the angle of polarization similar to that of clear skies," *J. Opt. Soc. Am. A*, 2007.

[2] I. Pomozi *et al.*, "How the clear-sky angle of polarization pattern continues underneath clouds: full-sky measurements and implications for animal orientation," *J. Exp. Biol.*, 2001.

[3] J. Gálet *et al.*, "Polarization patterns of the summer sky and its neutral points measured by full-sky imaging polarimetry in Finnish Lapland north of the Arctic Circle," *Proc. R. Soc. London, Ser. A*, 2001.

[4] K. J. Voss and Y. Liu, "Polarized radiance distribution measurements of skylight. I. System description and characterization," *Appl. Opt.*, 1997.

[5] Horva'th *et al.*, "First observation of the fourth netral polarization point in the atmosphere," *J. Opt. Soc. Am. A*, 2002.

[6] B. Suhai and G. Horva'th, "How well does the Rayleigh model describe the E-vector distribution of skylight in clear and cloudy conditions? A full-sky polarimetric study," *J. Opt. Soc. Am. A*, 2002.

[7] S. Rossel and R. Wehner, "The bee's map of the e-vector pattern in the sky," *Proc. Nati Acad. Sci. USA*, 1982.

[8] M. V. Berry *et al.*, "Polarization singularities in the clear sky," *New Journal of Physics*, 2004.

[9] Sabbah *et al.*, "Experimental and theoretical study of skylight polarization transmitted through Snell's window of a flat water surface," *J. Opt. Soc. Am. A*, 2006.

[10] J. H. Hannay, "Polarization of sky light from a canopy atmosphere," *New Journal of Physics*, 2004.

[11] D. Carruthers, C. Uloth, and G. G. Roy, "An evaluation of formulae for solar declination and the equation of time," *Research Report No. RR17, School of Architecture, the University of Western Australia*, Jan. 1990.

[12] D. Goldstein and G. Goldstein, *Polarized light*, 2003.